Effect of Zeeman coupling on the Majorana vortex modes in iron-based topological superconductors

Areg Ghazaryan, P. L. S. Lopes, Pavan Hosur, Matthew J. Gilbert, and Pouyan Ghaemi

Phys. Rev. B **101**, 020504 — Published 13 January 2020

DOI: 10.1103/PhysRevB.101.020504

Effect of Zeeman coupling on the Majorana vortex modes in iron-based topological superconductors

Areg Ghazaryan,[1] P. L. S. Lopes,[2] Pavan Hosur,[3] Matthew J. Gilbert,[4,5,6] and Pouyan Ghaemi[7,8]

[1] *IST Austria (Institute of Science and Technology Austria), Am Campus 1, 3400 Klosterneuburg, Austria*
[2] *Stewart Blusson Quantum Matter Institute, University of British Columbia, Vancouver, British Columbia, Canada V6T 1Z4*
[3] *Department of Physics, University of Houston, Houston, TX 77204, USA*
[4] *Micro and Nanotechnology Laboratory, University of Illinois at Urbana-Champaign, Urbana, Illinois 61801, USA*
[5] *Department of Electrical and Computer Engineering, University of Illinois at Urbana-Champaign, Urbana, Illinois 61801, USA*
[6] *Department of Electrical Engineering, Stanford University, Stanford, California 94305, USA*
[7] *Physics Department, City College of the City University of New York, New York, NY 10031, USA*
[8] *Graduate Center of the City University of New York, NY 10031, USA*

(Dated: January 6, 2020)

In the superconducting regime of $FeTe_{(1-x)}Se_x$, there exist two types of vortices which are distinct by the presence or absence of zero energy states in their core. To understand their origin, we examine the interplay of Zeeman coupling and superconducting pairings in three-dimensional metals with band inversion. Weak Zeeman fields are found to suppress the intra-orbital spin-singlet pairing, known to localize the states at the ends of the vortices on the surface. On the other hand, an orbital-triplet pairing is shown to be stable against Zeeman interactions, but leads to delocalized zero-energy Majorana modes which extend through the vortex. In contrast, the finite-energy vortex modes remain localized at the vortex ends even when the pairing is of orbital-triplet form. Phenomenologically, this manifests as an observed disappearance of zero-bias peaks within the cores of topological vortices upon increase of the applied magnetic field. The presence of magnetic impurities in $FeTe_{(1-x)}Se_x$, which are attracted to the vortices, would lead to such Zeeman-induced delocalization of Majorana modes in a fraction of vortices that capture a large enough number of magnetic impurities. Our results provide an explanation to the dichotomy between topological and non-topological vortices recently observed in $FeTe_{(1-x)}Se_x$.

Introduction: To date, one of the major impediments in the search for Majorana fermions (MFs) is the required intrinsic[1,2] or induced[3–6] topological superconductivity. Of the available materials that possess topology, superconductivity and magnetism, iron-based superconductors are of recent interest[7–15]. In particular, the $FeTe_{0.55}Se_{0.45}$ (FTS) has recently been shown to have the band inversion that results in a helical, topologically-protected, Dirac cone on the surface[16–19]. The phenomenology of vortices, proliferated in the presence of magnetic fields, is also noteworthy in FTS[20–23]. The low charge density in FTS is experimentally advantageous as it results in large Caroli-de Gennes-Matricon (CDM) vortex mode gaps[24] which facilitates the spectral detection of zero-energy vortex modes via scanning tunneling microscopy (STM).

While the evidence of MFs in FTS has been observed, a comprehensive understanding of the salient physics of the vortex composition is lacking. More precisely, the energy spectra of the vortices follow two different hierarchies relative to the CDM vortex gap, $\delta = \frac{\Delta^2}{\mu}$, where Δ is the bulk superconducting gap and μ is the chemical potential. The trivial vortex energy spectrum scales as $(n + 1/2)\delta$, (with $n \in \mathbb{Z}$) which does not include the zero mode, whereas the topological vortices follow $n\delta$. Additionally, the percentage of vortices with zero-energy modes decreases as the perpendicular magnetic field increases, even-though the inter-vortex distances are larger than the superconducting coherence length[20,21,25,26]. More over, the distribution of vortices with and without zero mode has no correlation with the charge disorder on the surface of the material[21]. These features, on aggregate, suggest that the properties that distinguish the two classes of vortices stem from the bulk properties of individual vortex rather than those of the surface states. In particular the effects of magnetic field, beyond generation of vortices, might crucially affect the properties of superconducting state and the vortices.

Motivated by experimental observations, we examine the effects of Zeeman coupling on the vortex modes in FTS. As the topological properties of FTS are driven by band inversion, we eschew more complex band models and utilize a simple model of a doped 3D time-reversal symmetric (TRS) topological insulator (TI) which has been used as an appropriate toy model to investigate the properties of vortices in FTS[27–29]. Due to the strong spin-orbit coupling, Zeeman field splits the the degenerate Fermi surface in TRS TI into two helical Fermi surfaces with opposite helicity[30]. In this letter, we show that the split Fermi surfaces prefer an orbital-triplet superconducting pairing which delocalizes the MF modes at the ends of the vortices on the surface. To make direct connection with the dichotomy of vortices in FTS we note that the Zeeman field would result from the magnetic impurities along the vortex core[31,32]. Interestingly, such magnetic Fe impurities are known to exists in FTS[33,34] and interact with the vortices[31]. In addition, increase of magnetic field naturally leads to enhancement of Zeeman

coupling which further destabilize the topological vortices, as is experimentally observed. We should also note that neutron scattering measurements have shown the evidence of ferromagnetic clusters of Fe atoms in FTS[33]. Therefore, the decrease of the concentration of the Fe impurities is directly linked to the increase of the fraction of topologicla vortices. Observation of the clusters of vortices, with and without zero energy vortex modes, would further support our theory.

Model Hamiltonian: The 3D TRS TI is represented by the tight-binding Hamiltonian $\mathcal{H}_{\mathbf{k}} = \sum_{\mathbf{k}} \psi^{\dagger}_{\mathbf{k}} \left[\tau_x \mathbf{d}_{\mathbf{k}}.\boldsymbol{\sigma} + m_{\mathbf{k}}\tau_z - \mu\right] \psi_{\mathbf{k}}$ where Pauli matrices σ_i and τ_i act on spin and orbital space respectively, $d_{k_i} = 2t\sin(k_i)$, $m_{\mathbf{k}} = M + m_0 \sum_i \cos(k_i)$ and M, m_0, t are parameters of the model and μ is the chemical potential. By varying the parameters, this model Hamiltonian represents both strong and week TRS TIs[35]. The tight-binding model is used for the numerical calculations while our analytical results are based on the effective model

$$\mathcal{H} = \hbar v_F \tau_x \boldsymbol{\sigma} \cdot \mathbf{k} + m_k \tau_z, \tag{1}$$

where $m_k = m + \epsilon k^2$ is the effective mass term and $\mathbf{k}$ is the momentum relative to the center of the Brillouin zone. The trivial (topological) insulator corresponds to $m\epsilon > 0$ (< 0). Without loss of generality, we take $\hbar v_F = 1$.

With the Hamiltonian defined, we begin our analysis in the metallic phase, when $\mu > |m|$. The model displays two degenerate Fermi surfaces that split by a Zeeman field Δ_Z. Since the bulk band structure gap is large compared with superconducting gap, we use the effective Hamiltonian resulting from projecting the Hamiltonian in Eq. (1) into the states at the two Fermi surfaces:

$$\mathcal{H} = \int d^3\mathbf{k} f^{\dagger}_{\mathbf{k}} \left[\left(E_{\mathbf{k}} - \mu\right)\nu_0 + \mathbf{d}_{\mathbf{k}} \cdot \boldsymbol{\nu}\right] f_{\mathbf{k}}. \tag{2}$$

Here ν_i are the identity or Pauli matrices acting on the the space of two Fermi surfaces. The vector $\mathbf{d}_{\mathbf{k}} = \frac{\Delta_Z}{2}\left(-\frac{m_{\mathbf{k}}}{E_{\mathbf{k}}}\frac{k_x^2+k_y^2}{|\mathbf{k}|},\ 0,\ \frac{k_z}{k}\right)$ represents the Zeeman field and $f_{\mathbf{k}}$ is the Fermion fields $\psi_{\mathbf{k}}$ projected onto the Fermi surfaces[30]. The two fermi spin-split fermi surfaces are identified by diagonalizing the projected Hamitonian (2) in the ν space.

Previous analysis[36] identified two types of superconductivity in doped TIs which are energetically favorable: intra-orbital spin singlet, $\int d^3\mathbf{r}\psi^{\dagger}\Delta i\tau_0\sigma_y\psi^{\dagger T} + H.c.$, and inter-orbital orbital-triplet spin-singlet, $\int d^2\mathbf{k}\psi^{\dagger}_{\mathbf{k}} i\tau_x\sigma_y\psi^{\dagger T}_{-\mathbf{k}} + H.c.$. Henceforth, we will refer to these superconducting pairings as intra-orbital singlet and inter-orbital triplet pairings, respectively.

Upon projection onto the Fermi surfaces the superconducting pairing potentials assume the following form,

$$\frac{\Delta_\alpha}{2}\int d^3\mathbf{k} f^{\dagger}_{\mathbf{k}} e^{-i\phi_{\mathbf{k}}}\nu_\alpha f^{\dagger T}_{-\mathbf{k}}, \tag{3}$$

where for the intra-orbital singlet pairing $\alpha = 1$ and for inter-orbital triplet pairing $\alpha = 0$. Examination of the superconducting pairing term in Eq. (3) in comparison with the kinetic Hamiltonian in Eq. (2) shows that the intra-orbital singlet pairing, Δ_1, corresponds to pairing electrons between different Zeeman split fermi surfaces. In contrast, the inter-orbital triplet pairing, Δ_0, pairs electrons solely within each of the Zeeman split Fermi surfaces. Thus, the effect of Zeeman coupling is to break the TRS within the model and imbalance the two pairing potentials in the favor of Δ_0 which couples the electrons solely within each Zeeman split Fermi surface[37].

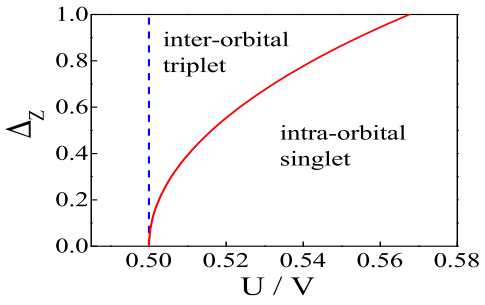

FIG. 1. Phase boundaries between regions with superconducting order parameters Δ_1 or Δ_0 as function of the ratio U/V of interaction strengths of each channel and the field magnitude, Δ_Z (Red solid curve). The blue dashed line is guide for the eye of the case when $\Delta_Z = 0$. The parameters of the Hamiltonian are $m = -0.5$ and $\epsilon = 0.5$. Increased Zeeman coupling results in larger regions where inter-orbital triplet pairing is the ground state.

To examine the outlined effect of Zeeman coupling on the dominant form of superconducting pairing, we utilize a linear gap equation[30] to determine the critical temperatures of the two superconducting pairings[36,38–40]. The corresponding $U - V$ model, in which U and V are the intra and inter orbital interaction, leads to the equation :

$$\det\begin{vmatrix} U\bar{\chi} - 1 & U\chi_2 \\ V\chi_2 & V\chi_1 - 1 \end{vmatrix} = 1, \qquad V\chi_0 = 1. \tag{4}$$

Here $\bar{\chi}$, χ_1 and χ_2 are the superconducting susceptibilities characterizing intra-orbital spin-singlet pairing and χ_0 describes the inter-orbital spin triplet pairing. $\bar{\chi} = -\int_{-w_D}^{w_D} \mathcal{D}(\xi)\tanh\left(\xi/2T\right)/2\xi d\xi$ is the standard s-wave susceptibility, $D(\xi)$ is the density of states and w_D is the Debye frequency.

By numerically solving the $U - V$ Eq. (4), we obtain the critical temperature T_c for each pairing channel. Fig. 1 shows the resulting phase boundaries that delineate the regions where either Δ_0 or Δ_1 correspond to higher critical temperature and so is the dominant form of pairing. In Fig. 1, we plot the phase boundary as we vary Δ_Z and the ratio U/V. It is evident in Fig. 1 that the inclusion of the Zeeman effect results in the enhancement of the triplet (Δ_0) pairing and the suppression of the singlet one (Δ_1) at a given chemical potential.

Vortex Modes: Having established the phase diagram of the superconducting pairing, we proceed to study the

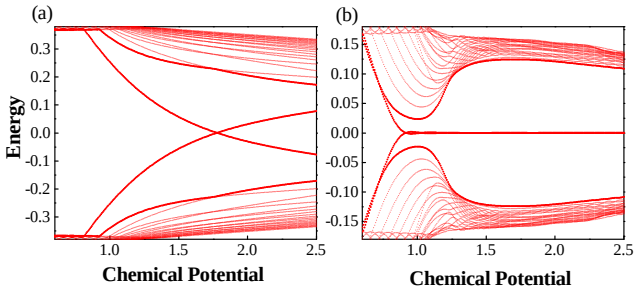

FIG. 2. Dependence of the vortex modes energies on the chemical potential μ obtained from the 3D lattice model with periodic boundary conditions along the z-direction for $k_z = 0$. (a) Intra-orbital singlet pairing $\Delta_1 = 0.4$ for $\Delta_Z = 0$. (b) Inter-orbital triplet pairing $\Delta_0 = 0.4$ and $\Delta_Z = 0.2$. The parameters for the model are: $M = 4.5$, $m_0 = -2.0$ and $t = 1.0$ with the calculation performed on a 48×48 lattice in the $x - y$ plane. We observe a zero-energy mode state exists for all chemical potentials inside the conduction band when the pairing is inter-orbital triplet type.

internal structure of the vortices as we insert a π-flux-tube into the pairing potential: $\Delta_\alpha(r) = |\Delta_\alpha(r)|e^{i\theta}$[41,42]. Since the coherence length FTS is in the range of $2 - 10\,\mathrm{nm}$[19,20,25] and the observed distance between vortices is around 30 nm for magnetic fields up to 6 T[21,22] we disregard inter-vortex hybridization effects and concentrate on the physical properties of single vortex. We fix $k_z = 0$ as we are interested in points where the topological $\mathbb{Z}_2$ index changes and this only occurs at $k_z = 0$ or π. Since the vortex modes stem from states close to the Fermi energy, their wave functions can be expressed in terms of a superposition of the TI conduction band eigenstates in cylindrical coordinates $\chi^{\nu}_{l,k}$[30]. Here ls are angular momentum quantum numbers and $\nu = \pm$ correspond to the two energy bands of Hamiltonian (1) which are split by Zeeman coupling.

Given the rotational symmetry of the vortex profile, the vortex modes with different ls do not hybridize and the vortex Hamiltonian decouples into sectors with fixed l. Also, for inter-orbital triplet pairing, the vortex does not mix the ν's. On the other hand[30], the translation symmetry in the plane perpendicular to the vortex is broken and different radial momenta k, as well as Nambu particle-hole states are mixed by the vortex. The effective vortex Hamiltonian acting in the radial momentum and Nambu particle-hole spaces takes the form of a 1D Jackiw-Rebbi model[43]

$$H^{\nu}_{l} = \Pi_z \frac{\Delta_0 \lambda_\nu(k)}{\xi_0} + \Pi_y \frac{\Delta_0}{\xi_0}(i\partial_k) + \Pi_x E^{\nu}_{l,0}(k). \qquad (5)$$

The Π matrices act on a Nambu space, ξ_0 is the superconducting coherence length and $\Delta_0\lambda_\nu(k)/\xi_0 = k + \frac{hm_{\mathbf{k}}}{2E^0_{\mathbf{k}}}\nu - \mu$. The Jackiw-Rebbi lowest-energy solutions are localized at the Fermi surface where the coefficient $\lambda_\nu(k^{\nu}_F)$ changes sign. These states have the form $e^{-\int_{k^{\nu}_F - k}^{k^{\nu}_F + k} dk' \lambda_\nu(k')}(1,1)^T$ in Nambu particle-hole basis and has energy $E^{\nu}_{l,0}(k_F)$. Notice that vortex-mode wave functions are exponentially localized around Fermi wavevector. Since the BdG Hamiltonian in equation (5) is in the bases of TI conduction band states, the full wave function of the two vortex modes (each associated with one Zeeman split Fermi surface) takes the form $\Psi^{\nu}_V(l,r) \approx \chi^{\nu}_{l,k_F}(r)(1,1)^T_\Pi$ where $(1,1)^T_\Pi$ is the spinor in Nambu particle-hole space. Previously, a similar result was obtained for the intra-orbital spin-singlet case[41,42]. In that case, solutions where again centered at the metallic phase Fermi surface, with corresponding energies $E^{\nu}_{l,1} = \frac{\Delta}{k_F\xi_1}(2\pi l + \pi + \nu\phi_B)$. ϕ_B is a Berry-phase-like term which permits zero-modes whenever $\phi_B = \pi$. In contrast, for the inter-orbital triplet case, the energies of the vortex modes are $E^{\nu}_{l,0} = \frac{\Delta_0}{k^{\nu}_F\xi_0}(2\pi l)$. Therefore, in the inter-orbital triplet case, a zero-energy channel exists *along* the vortex which delocalizes the MFs on the sample surface and suppresses the zero-bias signal in STM.

In Fig. 2 we verify the analytic results using a 3D lattice model with periodic boundary conditions along the z-direction. Fig. 2 (a) shows the spectrum of the vortex modes for the intra-orbital singlet pairing where the vortex gap closes solely when $\phi_B = \pi$. In contrast, Fig. 2 (b) shows that for the inter-orbital triplet pairing, once the chemical potential is in the conduction band the system develops vortex zero modes which remain gapless for all chemical potentials. Thus, increasing the Zeeman coupling results in a shift of the Fermi surfaces that destabilize the intra-orbital singlet pairing in favor of the inter-orbital triplet pairing leading to the omnipresence of a zero mode in the vortex core.

In Fig. 3, we examine the manifestation of the change in superconducting pairing by inserting a vortex in the tight-binding lattice model. We set $\mu = 1.1t$, where t is hoping amplitude in the lattice model. For small Zeeman couping, the intra-orbital singlet channel is dominant and the MFs are localized at the ends of the vortex on the surface. As the Zeeman splitting is increased, we destabilize the intra-orbital singlet pairing channel in favor of the inter-orbital triplet pairing allowing MFs to penetrate into the bulk. At sufficiently high Zeeman coupling, the intra-orital singlet pairing is fully suppressed and MFs on the surface delocalize through the vortex modes and extend into the bulk of the superconductor. As will be shown below, this mechanism would only delocalize the Majorana zero modes and not the finite energy states.

Effective 1D Vortex Model: Using the vortex mode wavefunctions $\Psi^{\nu}_V(l,r)$, we now derive an effective Hamiltonian for the modes along the vortex line connecting the sample surfaces [44]. To this end, we calculate the matrix elements of the k_z-dependent terms in Hamiltonian, Eq. (1), within the space of the two families of vortex modes $\Psi^{\nu}_V(l,r)$. Defining η_i as Pauli matrices acting on the space of the two sets of modes, the effective

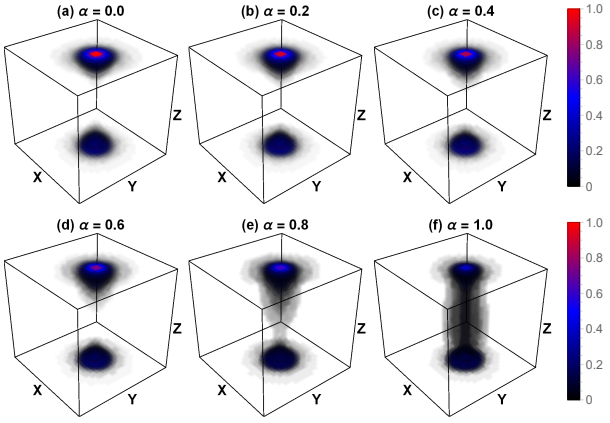

FIG. 3. Spatial profile of the lowest energy vortex mode in 3D slab geometry for different values of parameter α, which controls the amplitude of the inter-orbital triplet pairing $\Delta_0 = \alpha\Delta_0^0$, intra-orbital s-wave $\Delta_1 = (1-\alpha)\Delta_1^0$ and Zeeman field $\Delta_Z = \alpha\Delta_Z^0$ around the vortex. The calculation is performed on a $24\times24\times24$. The parameters used are: $\mu = 1.1$, $\Delta_0^0 = 0.4$, $\Delta_1^0 = 0.4$, $\Delta_Z^0 = 0.2$, $M = 4.5$, $m_0 = -2.0$ and $t = 1.0$.

vortex Hamiltonians have the general form

$$H_V^l(k_z) = \frac{E_l^+ + E_l^-}{2}\eta_0 + \left(\frac{E_l^+ - E_l^-}{2} + \tilde{\epsilon}_l k_z^2\right)\eta_z - \tilde{v}_z k_z \eta_x \tag{6}$$

Here, E_l^ν are the energies of l-th vortex modes coming from the Fermi surface corresponding to $\nu = \pm$ and increase monotonically with l for fixed ν. $\tilde{\epsilon}_l$ and $\tilde{v}_z$ are parameters of the k_z-dependent terms, projected into the lth vortex mode. Nambu particle-hole symmetry is given by $\mathcal{P}^{-1}[H_V^l(k_z)]\mathcal{P} = H_V^{-l}(-k_z) = -H_V^l(k_z)$, which implies $E_{-l}^\pm = -E_l^\pm$ and $\tilde{\epsilon}_l = -\tilde{\epsilon}_{-l}$ as shown in[30]. For each $l \neq 0$, Eq. (6) realizes a Z_2 topological state with modes with angular momentum l localized at the ends of the vortex and finite energy if $\left(E_l^+ - E_l^-\right)\tilde{\epsilon}_l < 0$[45]. Since the Zeeman field is along the flux line we have $k_F^+ < k_F^-$, which implies $\mathrm{sgn}(E_l^+ - E_l^-) = \mathrm{sgn}(l)$ and reduces the above condition to $\epsilon < 0$; this is true for FTS, whose normal state corresponds to a doped TI. The particle-hole partner of these states corresponds to angular momentum $-l$. The perturbations could modify the energy of these modes in pair such that particle-hole symmetry is respected.

In contrast, Nambu particle-hole symmetry implies $E_0^\pm = 0$ as well as $\epsilon_0 = 0$, so the vortex is gapless when the pairing is purely of inter-orbital triplet form. As shown in Fig. 4(b), the effective vortex Hamiltonian for the zero energy states is linearly dispersing with momentum along the vortex. However, Nambu symmetry permits a mass term $\propto \eta_y$; indeed, the remnant singlet pairing outside of the vortex induces the scattering between vortex modes coming from different Fermi surfaces, producing a term $\eta_y\Delta_s^{Vrx}$[30]. Δ_s^{Vrx} is k_z-independent, thus making the vortex topologically *trivial* and devoid of zero modes at its ends.

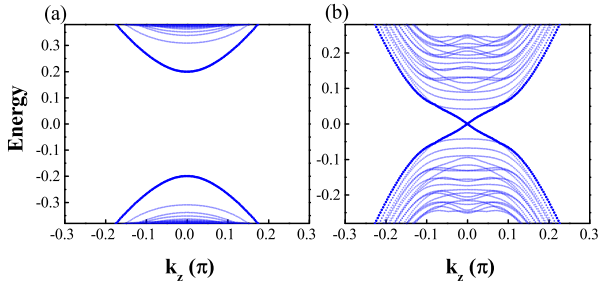

FIG. 4. k_z momentum dependence of the vortex modes for (a) intra-orbital s-wave pairing $\Delta_1 = 0.4$ and (b) inter-orbital triplet pairing $\Delta_0 = 0.4$ with $\Delta_Z = 0.2$ and the chemical potential set to be $\mu = 1.1$. Additional parameters of the model are the same as in Fig. 2.

We note that the energy levels at the vortex ends, ε_l, are equally spaced and are labeled by integers l which corresponds to angular momentum associated with the rotational symmetry of the vortex. The only patterns for such vortex mode energies that are consistent with particle-hole symmetry are $\varepsilon_l \propto l$ and $\varepsilon_l \propto l + 1/2$. The former contains a zero mode while the latter does not. Since, as argued above, the vortex is topologically trivial and lacks zero modes at its ends when the Zeeman-driven orbital-triplet pairing dominates, $\varepsilon_l \propto l+1/2$ in this case. On the other hand, if the intra-orbital singlet pairing dominates, the vortex ends up being topological and its ends have a spectrum containing the zero modes[41] and satisfies $\varepsilon_l \propto l$. These results are in accordance with the two types of vortex spectra seen in reference[22].

A Zeeman coupling in the vortex regions can be mediated by the magnetic impurities present along the vortex. For such effect to have notable experimental signature, however, it is crucial for the vortices to be attracted to the magnetic atoms. The comparison of energies of states where the vortices are far from the the magnetic impurities with the case where vortex is passing through the impurity is the direct method to examine the vortex impurity interactions. In addition to the surface tension of a vortex, the energy of in-gap Shiba states at the magnetic impurity site[46–48] and the CDM modes define the energy cost of the vortex creation. A recent study directly compared the energy of these in gap states for the case where the vortex and impurity are at the same location with the energy for the isolated vortex and impurity[31]. This study, which was performed for strongly spin-orbit coupled materials and aimed to study the effect of magnetic impurities in FTS, showed that the the sum of the energy of the CDM and Shiba modes decreases when the vortex passes through the impurity. This general reduction in energy resulting from placing a vortex on the impurity provides a strong suggestion for the attractive interaction between vortices and impurities. The result of this attraction motivate our considerations which, as seen, leads to a depiction of the FTS vortex phenomenology in accordance with experimental data, without the need to

invoke MF hybridizations.

Conclusion: We have examined the effect of Zeeman coupling on the structure of vortex modes in FTS. We find that intra-orbital singlet pairing, which support MFs at the ends of the vortices, is supperessed by Zeeman field and is replaced with the inter-orbital triplet paring, with only finite energy vortex modes at the ends of vortex.

The property of the FTS that facilitate our models is the degenerate Fermi surfaces that are split into two helical Fermi surfaces by the Zeeman field. The size of the superconducting gap in FTS is of the order of 2.5 meV for hole pocket and 4.2 meV for electron pocket[18,33,34] and the size of the Fe impurities dipole-moments of the order of $5\mu_B$[31,33]. Given the average distance of the Fe impurity atoms, their associated Zeeman coupling is of the order of $\Delta_Z \approx 7.84\,\text{meV}$. It is then evident that the Zeeman coupling can affect the form of the superconducting paring. We demonstrate that the nature of the vortices in FTS is inextricably linked to the effect of Zeeman coupling, which determines the form of superconducting pairing and indicates that suppression of Zeeman coupling, by reduction of magnetic impurities, stabilizes the vortex MFs in FTS. The importance of our proposed mechanism can be checked by observation of the effect of the density of the magnetic impurities on the fraction of vortices with MF vortex modes.

Acknowledgments. This research was supported under National Science Foundation Grants EFRI-1542863, DMR-1824265 and PSC-CUNY Award, jointly funded by The Professional Staff Congress and The City University of New York (PG). PLSL is supported by the Canada First Research Excellence Fund. AG is support by the European Unions Horizon 2020 research and innovation program under the Marie Skodowska-Curie grant agreement No 754411. PH was supported by the Department of Physics and the College of Natural Sciences and Mathematics at the University of Houston. M.J.G. acknowledges financial support from the National Science Foundation (NSF) under Grant No. DMR-1720633, CAREER Award ECCS-1351871 and the Office of Naval Research (ONR) under grant N00014-17-1-3012.

[1] Y. Li and Z.-A. Xu, Advanced Quantum Technologies , 1800112.
[2] M. Sato and Y. Ando, Reports on Progress in Physics **80**, 076501 (2017).
[3] L. Fu and C. L. Kane, Phys. Rev. Lett. **100**, 096407 (2008).
[4] R. M. Lutchyn, J. D. Sau, and S. Das Sarma, Phys. Rev. Lett. **105**, 077001 (2010).
[5] V. Mourik, K. Zuo, S. Frolov, S. Plissard, E. Bakkers, and L. Kouwenhoven, Science **336**, 1003 (2012).
[6] S. Nadj-Perge, I. K. Drozdov, J. Li, H. Chen, S. Jeon, J. Seo, A. H. MacDonald, B. A. Bernevig, and A. Yazdani, Science **346**, 602 (2014).
[7] N. Hao and J. Hu, National Science Review **6**, 213 (2018).
[8] P. Dai, Rev. Mod. Phys. **87**, 855 (2015).
[9] R. P. Day, G. Levy, M. Michiardi, B. Zwartsenberg, M. Zonno, F. Ji, E. Razzoli, F. Boschini, S. Chi, R. Liang, P. K. Das, I. Vobornik, J. Fujii, W. N. Hardy, D. A. Bonn, I. S. Elfimov, and A. Damascelli, Phys. Rev. Lett. **121**, 076401 (2018).
[10] M. H. Christensen, J. Kang, and R. M. Fernandes, Phys. Rev. B **100**, 014512 (2019).
[11] V. Cvetkovic and O. Vafek, Phys. Rev. B **88**, 134510 (2013).
[12] A. Lau and C. Timm, Phys. Rev. B **90**, 024517 (2014).
[13] C. Youmans, A. Ghazaryan, M. Kargarian, and P. Ghaemi, Phys. Rev. B **98**, 144517 (2018).
[14] E. J. König and P. Coleman, Phys. Rev. Lett. **122**, 207001 (2019).
[15] R.-X. Zhang, W. S. Cole, X. Wu, and S. D. Sarma, Phys. Rev. Lett. **123**, 167001 (2019).
[16] T. Hanaguri, S. Niitaka, K. Kuroki, and H. Takag, Science **328**, 474 (2010).
[17] Z. Wang, P. Zhang, G. Xu, L. K. Zeng, H. Miao, X. Xu, T. Qian, H. Weng, P. Richard, A. V. Fedorov, H. Ding, X. Dai, and Z. Fang, Phys. Rev. B **92**, 115119 (2015).
[18] P. Zhang, K. Yaji, T. Hashimoto, Y. Ota, T. Kondo, K. Okazaki, Z. Wang, J. Wen, G. D. Gu, H. Ding, and S. Shin, Science **360**, 182 (2018).
[19] G. Xu, B. Lian, P. Tang, X.-L. Qi, and S.-C. Zhang, Phys. Rev. Lett. **117**, 047001 (2016).
[20] D. Wang, L. Kong, P. Fan, H. Chen, S. Zhu, W. Liu, L. Cao, Y. Sun, S. Du, J. Schneeloch, R. Zhong, G. Gu, L. Fu, H. Ding, and H.-J. Gao, Science **362**, 333 (2018).
[21] T. Machida, Y. Sun, S. Pyon, S. Takeda, Y. Kohsaka, T. Hanaguri, T. Sasagawa, and T. Tamegai, Nature materials **18**, 811 (2019).
[22] L. Kong, S. Zhu, M. Papaj, H. Chen, L. Cao, H. Isobe, Y. Xing, W. Liu, D. Wang, P. Fan, Y. Sun, S. Du, J. Schneeloch, R. Zhong, G. Gu, L. Fu, H.-J. Gao, and H. Ding, Nature Physics **15**, 1181 (2019).
[23] S. Zhu, L. Kong, L. Cao, H. Chen, S. Du, Y. Xing, D. Wang, C. Shen, F. Yang, J. Schneeloch, R. Zhong, G. Gu, L. Fu, Y.-Y. Zhang, H. Ding, and H.-J. Gao, ArXiv:1904.06124.
[24] C. Caroli, P. D. Gennes, and J. Matricon, Physics Letters **9**, 307 (1964).
[25] H. Lei, R. Hu, E. Choi, J. Warren, and C. Petrovic, Phys. Rev. B **81**, 094518 (2010).
[26] C.-K. Chiu, Y. H. T. Machida, T. Hanaguri, and F.-C. Zhang, "Scalable majorana vortex modes in iron-based superconductors," (2019), arXiv:1904.13374.
[27] S. Qin, L. Hu, X. Wu, X. Dai, C. Fang, F.-C. Zhang, and J. Hu, Science Bulletin **64**, 1207 (2019).
[28] R.-X. Zhang, W. S. Cole, and S. D. Sarma, Phys. Rev. Lett. **122**, 187001 (2019).
[29] P. Zhang, Z. Wang, X. Wu, K. Yaji, Y. Ishida, Y. Kohama, G. Dai, Y. Sun, C. Bareille, K. Kuroda, T. Kondo, K. Okazaki, K. Kindo, X. Wang, C. Jin, J. Hu, R. Thomale, K. Sumida, S. Wu, K. Miyamoto, T. Okuda, H. Ding, G. D. Gu, T. Tamegai, T. Kawakami, M. Sato, and S. Shin, Nature Physics **15**, 41 (2019).
[30] See supplementary materials at [URL] for detailed calcuations.
[31] K. Jiang, X. Dai, and Z. Wang, Phys. Rev. X **9**, 011033

(2019).
[32] N.Zaki, G.Gu, A.M.Tsvelik, C.Wu, and P.D.Johnson, (2019), arXiv:1907.11602.
[33] V. Thampy, J. Kang, J. A. Rodriguez-Rivera, W. Bao, A. T. Savici, J. Hu, T. J. Liu, B. Qian, D. Fobes, Z. Q. Mao, C. B. Fu, W. C. Chen, Q. Ye, R. W. Erwin, T. R. Gentile, Z. Tesanovic, and C. Broholm, Phys. Rev. Lett. **108**, 107002 (2012).
[34] J.-X. Yin, Z. Wu, J.-H. Wang, Z.-Y. Ye, J. Gong, X.-Y. Hou, L. Shan, A. Li, X.-J. Liang, X.-X. Wu, J. Li, C.-S. Ting, Z.-Q. Wang, J.-P. Hu, P.-H. Hor, H. Ding, and S. H. Pan, Nature Physics **11**, 543 EP (2015).
[35] P. Hosur, S. Ryu, and A. Vishwanath, Phys. Rev. B **81**, 045120 (2010).
[36] L. Fu and E. Berg, Phys. Rev. Lett. **105**, 097001 (2010).
[37] Y. Kim, T. M. Philip, M. J. Park, and M. J. Gilbert, Phys. Rev. B **94**, 235434 (2016).
[38] S. Nakosai, Y. Tanaka, and N. Nagaosa, Phys. Rev. Lett. **108**, 147003 (2012).
[39] T. Hashimoto, S. Kobayashi, Y. Tanaka, and M. Sato, Phys. Rev. B **94**, 014510 (2016).
[40] P. Hosur, X. Dai, Z. Fang, and X.-L. Qi, Phys. Rev. B **90**, 045130 (2014).
[41] P. Hosur, P. Ghaemi, R. S. K. Mong, and A. Vishwanath, Phys. Rev. Lett. **107**, 097001 (2011).
[42] C.-K. Chiu, M. J. Gilbert, and T. L. Hughes, Phys. Rev. B **84**, 144507 (2011).
[43] R. Jackiw and C. Rebbi, Phys. Rev. D **13**, 3398 (1976).
[44] P. L. e. S. Lopes and P. Ghaemi, Phys. Rev. B **92**, 064518 (2015).
[45] X.-L. Qi and S.-C. Zhang, Rev. Mod. Phys. **83**, 1057 (2011).
[46] L. Yu, Acta Phys. Sin. **21**, 75 (1965).
[47] H. Shiba, Classical Spins in Superconductors **40**, 435 (1968).
[48] A. I. Rusinov, JETP Lett. **9**, 85 (1969).